

Isospin equilibration in multinucleon transfer reaction at near-barrier energies

Cheng Li,^{1,2,*} Cheikh A. T. Sokhna,^{1,2} Xinxin Xu,^{1,2} Jingjing Li,^{1,2} Gen Zhang,^{1,2} Bing Li,^{1,2} Zhishuai Ge,^{1,2} and Feng-Shou Zhang^{1,2,3,†}

¹*Beijing Radiation Center, Beijing 100875, China*

²*Key Laboratory of Beam Technology of Ministry of Education, College of Nuclear Science and Technology, Beijing Normal University, Beijing 100875, China*

³*Center of Theoretical Nuclear Physics, National Laboratory of Heavy Ion Accelerator of Lanzhou, Lanzhou 730000, China*



(Received 19 June 2018; revised manuscript received 19 January 2019; published 29 March 2019)

The isospin equilibration process in multinucleon transfer reactions is investigated by using the improved quantum molecular dynamics model. The collisions of $^{124}\text{Xe} + ^{208}\text{Pb}$ at near-barrier energy are studied with different symmetry energy coefficients. We find that the neutron transfer is enhanced at the early stages of the collisions under the strong symmetry potential. The neutron's transfer takes place at an earlier stage than the proton's. The trajectory of neutron flow is along the low-density path from the target to projectile. The average N/Z values of the primary products in the $^{58}\text{Ni} + ^{208}\text{Pb}$ reaction are also investigated and compared with available experimental data. It shows that the average N/Z values of the projectile-like products increase rapidly with increasing mass transfer. In the quasielastic collisions, the isospin equilibration process is incomplete due to a short contact time between the reaction partners. The complete isospin equilibration events take place in symmetric quasifission reactions.

DOI: [10.1103/PhysRevC.99.034619](https://doi.org/10.1103/PhysRevC.99.034619)

I. INTRODUCTION

The isospin transport effects in heavy-ion collisions have been studied for many years [1–9]. They include two different facets, named isospin diffusion and drift. The isospin diffusion is related to the isospin asymmetry of a system in which the projectile and target have different N/Z values [10]. The isospin drift is related to the density gradient which is expected to exist in the low-density neck region, even between two identical nuclei [11]. In the nuclear reactions, the isospin transport is initiated and continues until the system disintegrates or the chemical potentials for neutrons and protons in both nuclei become equal. If the interaction time between the projectile and target is long enough, the system will reach the situation of isospin equilibration.

In heavy-ion collisions at intermediate energies, isospin transport effects have been investigated in midperipheral collisions by analyzing the N/Z values of the reconstructed primary quasiprojectile, quasitarget, and midvelocity sources. Such as in the $^{40}\text{Ca} + ^{48}\text{Ca}$ reaction [3], one sees that the isospin diffusion effects lead to an increase of the N/Z of the quasiprojectile source. In the collisions of two identical N/Z values' nuclei (such as $^{58}\text{Ni} + ^{58}\text{Ni}$ [11]), it allows us to observe the isospin drift phenomenon without contamination from the midvelocity source.

At low incident energies, the multinucleon transfer (MNT) reaction is one of the most important mechanisms, which has attracted widespread interests in recent years both ex-

perimentally [12–22] and theoretically [23–35]. Unlike at the intermediate incident energies, the collisions between the reaction partners are not violent. The major products in MNT reactions only contain the quasiprojectile and the quasitarget fragments with the number of nucleon transfers up to 30 or more. No midvelocity fragments are formed. In general, the MNT reactions include the quasielastic, the deep-inelastic, and the quasifission reactions. These reaction mechanisms can be distinguished by analyzing the total-kinetic-energy-mass (TKE-Mass) distributions combined with the total kinetic energy loss (TKEL) distributions of the products [36–38]. The contact times between the reaction partners for the quasielastic, the deep-inelastic, and the quasifission reactions are quite different. The MNT reactions provide an opportunity to study the isospin equilibration process under different time scales. In the quasifission reactions, the typical time scales can reach 10^{-21} s order of magnitude or longer [39,40]. In this case, the nucleon transfer process may lead to a uniform distribution of the N/Z ratio.

Many experiments about the isospin equilibration effects at low energies have been performed by analyzing the N/Z values of reconstructed primary products during the last decades [18,41–43]. For example, the reactions of $^{64}\text{Ni} + ^{130}\text{Te}$ at $E_{\text{lab}} = 275$ MeV and $^{58}\text{Ni} + ^{208}\text{Pb}$ at $E_{\text{lab}} = 345$ MeV have been investigated by Królas *et al.* at Laboratori Nazionali di Legnaro (INFN) [18]. It is found that the isospin equilibration process is closely related to the number of nucleon transfers between the reaction partners. Actually, it is difficult to divide the contributions of the isospin diffusion and drift at low energies separately. Isospin equilibration is one important mechanism in MNT reactions, which is one promising approach to produce new neutron-rich nuclei. For example, the new

*licheng@mail.bnu.edu.cn

†Corresponding author: fszhang@bnu.edu.cn

isotopes ^{54}Ti , ^{56}V , $^{58,59}\text{Cr}$, ^{61}Mn , and $^{63,64}\text{Fe}$ were produced by Guerreau *et al.* through a 340 MeV ^{40}Ar beam accelerated by the Orsay ALICE accelerator facility bombarding on a ^{238}U target [44].

The neck is an important characteristic in MNT reactions, even in the early stages of the fusion reaction. It is formed in the dinuclear system and is characterized by subsaturation densities. The isospin transport and the energy dissipation processes of the system are closely related to the nucleon transfer between the reaction partners through the neck. The dynamical calculation is required to understand some details of these processes. A microscopic dynamics model, the improved quantum molecular dynamics (ImQMD) model [45,46], describes the nuclear reactions based on an effective nucleon-nucleon interaction. The ImQMD model is self-consistent for describing the behavior of neck evolution and nucleon transport during the collisions. In this work, we apply the ImQMD model to investigate the isospin equilibration process in the reactions of $^{124}\text{Xe} + ^{208}\text{Pb}$ and $^{58}\text{Ni} + ^{208}\text{Pb}$ at near-barrier energies.

The structure of this paper is as follows. In Sec. II, we briefly introduce the ImQMD model. The results and discussion are presented in Sec. III. Finally, the conclusion is given in Sec. IV.

II. THE MODEL

The ImQMD model is an improved version of the quantum molecular dynamics (QMD) model [47]. The standard Skyrme interaction with the omission of the spin-orbit term is adopted for describing the bulk and surface properties of nuclei [45]. The stochastic two-body collision process is added to the time evolution by the Hamilton equation of motion. To describe the fermionic nature of the N -body system, the Fermi constraint proposed by Papa *et al.* in the constrained molecular dynamics (CoMD) model [48,49] is introduced. It improves greatly the stability of an individual nucleus. The final state of the two-body collision process is checked so that it obeys the Pauli principle. Detailed descriptions of the ImQMD model can be found in Refs. [45,46]. The nuclear interaction potential can be read as

$$V_{\text{loc}} = \frac{\alpha}{2} \frac{\rho^2}{\rho_0} + \frac{\beta}{\gamma+1} \frac{\rho^{\gamma+1}}{\rho_0^\gamma} + \frac{g_{\text{sur}}}{2\rho_0} (\nabla\rho)^2 + \frac{C_s}{2\rho_0} (\rho^2 - \kappa_s (\nabla\rho)^2) \delta^2 + g_\tau \frac{\rho^{\eta+1}}{\rho_0^\eta}. \quad (1)$$

Here, $\rho = \rho_n + \rho_p$ is the nucleon density. $\delta = (\rho_n - \rho_p)/(\rho_n + \rho_p)$ is the isospin asymmetry. The first three terms in the above expression are obtained from the potential energy functional of the Skyrme interaction directly. The fourth term is the symmetry potential energy including the bulk and the surface symmetry potential energies. The surface symmetry potential energy term is related to the density gradient which is important for describing the neutron skin of nuclei. The last term is a small correction term. The density distribution

TABLE I. The model parameters (IQ2) adopted in this work.

α (MeV)	β (MeV)	γ	g_{sur} (MeV fm 2)	g_τ (MeV)	η	C_s (MeV)	κ_s (fm 2)	ρ_0 (fm $^{-3}$)
-356	303	7/6	7.0	12.5	2/3	32.0	0.08	0.165

function ρ of a system can be written as

$$\rho(r) = \sum_i \frac{1}{(2\pi\sigma_r)^{3/2}} \exp\left[-\frac{(\mathbf{r} - \mathbf{r}_i)^2}{2\sigma_r^2}\right]. \quad (2)$$

σ_r is the wave-packet width of the nucleon in coordinate space. The IQ2 parameter sets (see Table I) adopted in this work are the same as in Refs. [24,32]. The incompressibility coefficient, K_∞ , is 195 MeV. These parameter sets have been successfully applied on the heavy-ion collisions in fusion reactions [46,50], multinucleon transfer reactions [24,32], and ternary breakup reactions [51].

In this work, we set the z axis as the beam direction and the x axis as the impact parameter direction. We set the wave-packet width $\sigma_r = 1.3$ fm to calculate the isospin equilibration process of $^{124}\text{Xe} + ^{208}\text{Pb}$ and $^{58}\text{Ni} + ^{208}\text{Pb}$. The initial distance of the center of mass between the projectile and target is 30 fm.

III. RESULTS AND DISCUSSION

We first test the ImQMD model for the description of the MNT reactions. The collisions of $^{58}\text{Ni} + ^{208}\text{Pb}$ at $E_{\text{lab}} = 328.4$ MeV are simulated by using the ImQMD model. 39 000 simulation events are calculated with impact parameters from 0 to b_{\max} fm. $b_{\max} = R_P + R_T$, where R_P and R_T denote the radius of the projectile and the target, respectively. For each event, we simulate the collision process until $t = 2000$ fm/c with a step size of $\Delta t = 1$ fm/c. Figure 1 shows the isotope production cross sections from Mn to Ni. The fusion and elastic scattering events are not taken into account. The experimental data are taken from Ref. [52]. Thick folding lines and thick solid lines denote the calculations from the combination of the ImQMD+GEMINI and GRAZING models [53–55] with inclusion of the evaporation, respectively. The nuclear level densities in the GEMINI code [56] are taken as a Fermi-gas form with default parameters. From Fig. 1 we find that the measured isotope distributions for the elements Co and Ni can be reasonably reproduced by the ImQMD+GEMINI calculations. The discrepancy between the data and the calculations increases with the increasing number of proton transfer. The GRAZING calculations also show a similar behavior.

For simplicity, we consider head-on collisions of $^{124}\text{Xe} + ^{208}\text{Pb}$ at $E_{\text{c.m.}} = 450$ MeV to investigate the isospin equilibration process. For this reaction, the incident energy is slightly higher than the Coulomb barrier. It is almost impossible to form a compound nucleus, due to the large $Z_P Z_T$ value. The typical reaction process is that the colliding nuclei exchange a number of nucleons and then reseparate. Figure 2 shows the single-particle potentials of neutrons and protons in $^{124}\text{Xe} + ^{208}\text{Pb}$ along the beam direction at $t = 200$ and 300 fm/c. The single-particle potential is defined as $V_{sp}^q(\mathbf{r}) = \int \rho(\mathbf{r}') V(\mathbf{r}' -$

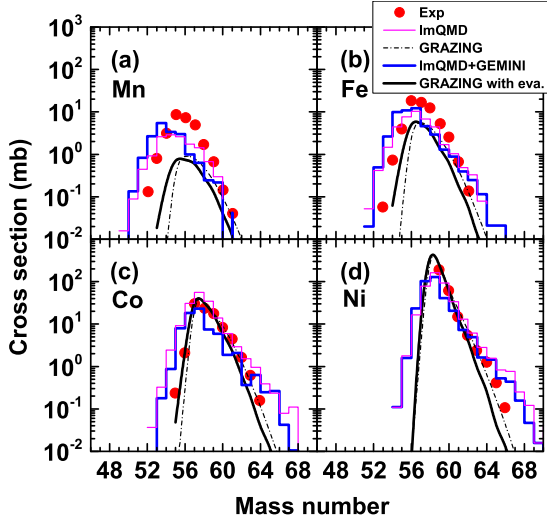


FIG. 1. Isotope production cross sections from Mn to Ni in the reaction of $^{58}\text{Ni} + ^{208}\text{Pb}$ at $E_{\text{lab}} = 328.4$ MeV. The thick folding lines and thick solid lines denote the calculations from the combination of the ImQMD+GEMINI and GRAZING models with the inclusion of evaporation, respectively. The thin folding lines and thin dash-dotted lines denote the primary fragment distributions from the ImQMD and GRAZING models, respectively. The experimental data (solid circles) are taken from Ref. [52].

$\mathbf{r}')d\mathbf{r}'$, where $q = n, p$, $\rho(\mathbf{r})$ is the density distribution of the system, and $V(\mathbf{r} - \mathbf{r}')$ is the effective nucleon-nucleon interaction. The Coulomb interaction is very important for the isospin transport processes in the early stages of the MNT reactions. For example, at $t = 200$ fm/c, the neutron transfer is allowed due to a lower barrier between the two reaction partners [see Fig. 2(a)]. However, for protons, the proton transfer between two reaction partners is forbidden at this

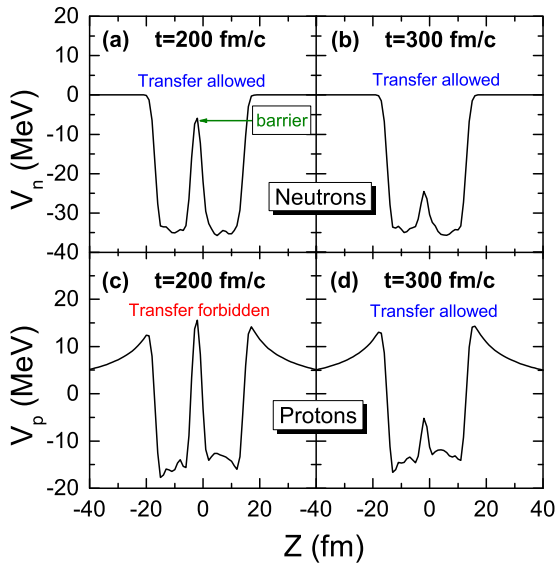


FIG. 2. The single-particle potentials of neutrons (top panels) and protons (bottom panels) in $^{124}\text{Xe} + ^{208}\text{Pb}$ at $t = 200$ and $t = 300$ fm/c.

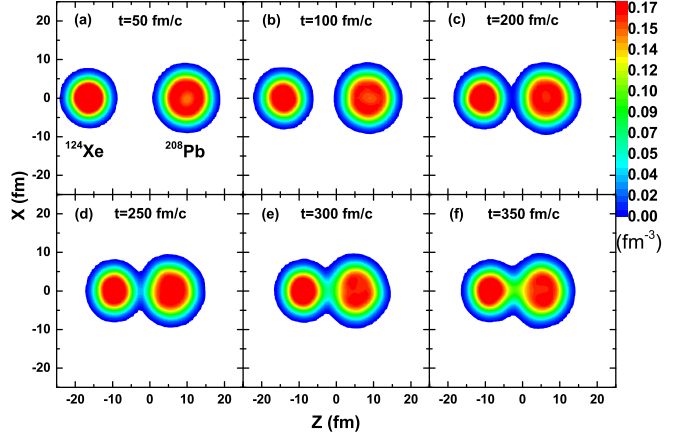


FIG. 3. Time evolution of the density profiles for $^{124}\text{Xe} + ^{208}\text{Pb}$ at $E_{\text{c.m.}} = 450$ MeV.

time because the barrier is very high [see Fig. 2(c)]. Hence, the neutron's transfer process takes place at an earlier stage than the proton's in the MNT reactions. At $t = 300$ fm/c, the barriers between the reaction partners are reduced both for neutrons and protons. Therefore, both neutrons and protons are allowed to transfer between the target and projectile [see Figs. 2(b) and 2(d)].

Figure 3 shows the time evolution of the density profiles for $^{124}\text{Xe} + ^{208}\text{Pb}$ at $E_{\text{c.m.}} = 450$ MeV. As seen from the figure, the central densities of the nuclei in the reactions are reasonable. In addition, we note that the diffuseness of the density can be seen clearly on the surface of the system. In Fig. 4, we show the contour plots of isospin asymmetry [$\delta = (\rho_n - \rho_p)/(\rho_n + \rho_p)$] for $^{124}\text{Xe} + ^{208}\text{Pb}$ during the evolution of the system. The average values of the isospin asymmetry for ^{124}Xe and ^{208}Pb nuclei are 0.13 and 0.21, respectively. From Fig. 4, one sees that the distributions of the isospin asymmetry in the cores of two reaction partners are uniform. The corresponding values of δ in the quasiprojectile and quasitarget are 0.1 and 0.17, respectively. However, the values of the isospin asymmetry on the surface of the nuclei are

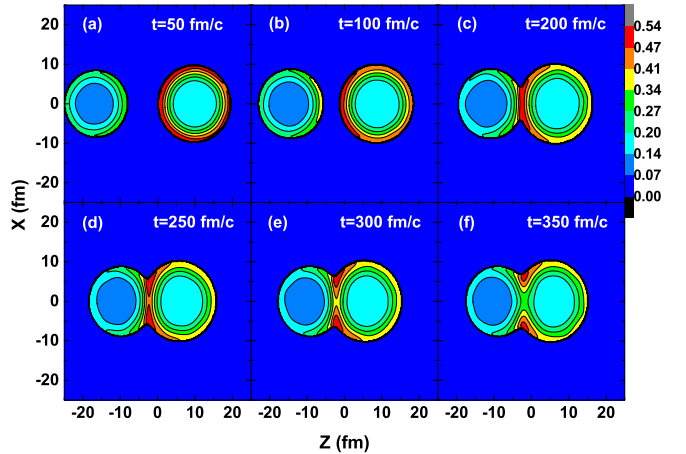


FIG. 4. Time evolution of the isospin asymmetry $\delta = (\rho_n - \rho_p)/(\rho_n + \rho_p)$ distributions for $^{124}\text{Xe} + ^{208}\text{Pb}$ at $E_{\text{c.m.}} = 450$ MeV.

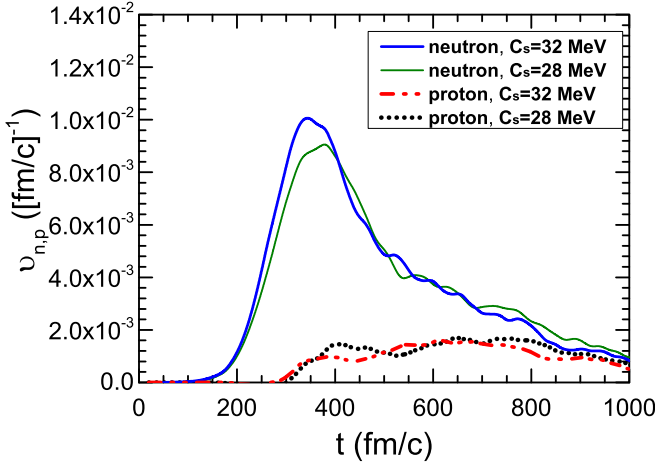


FIG. 5. The transfer coefficients for the neutron and proton with symmetry energy coefficients of $C_s = 28$ and 32 MeV in the head-on collisions of $^{124}\text{Xe} + ^{208}\text{Pb}$ at $E_{\text{c.m.}} = 450$ MeV.

significantly larger than those in the cores. The core of ^{208}Pb is covered by the neutron skin with maximal $\delta = 0.54$ at $t = 50$ fm/ c . The neutron enrichment can also be seen clearly in the low-density neck region. This phenomenon is known as the isospin drift which is due to the density gradient. The neutrons are preferably driven to the low density area [11]. In Fig. 4, one also can see that the neutron flow in the reactions is formed along the low-density path.

In order to investigate the isospin transport during the evolution of the dinuclear system, we introduce the separation plane to divide the quasiprojectile and quasitarget nuclei. The separation plane can be defined as the plane at the position where isocontours of the projectile and target densities cross each other. This method was adopted by the TDHF calculations in Refs. [57,58]. Figure 5 shows the transfer coefficients of the neutron and proton in the head-on collisions of $^{124}\text{Xe} + ^{208}\text{Pb}$ with the symmetry energy coefficients of $C_s = 28$ and 32 MeV. The transfer coefficient can be written as $v_{n,p} = dN_{n,p}/dt$, where $N_{n,p}$ denotes the net neutron or proton flux through the separation plane. The direction of nucleon transfer is from the target to projectile. One can see that the neutron transfer is enhanced in the case of $C_s = 32$ MeV at the early stages of the collisions due to the strong symmetry potential. The corresponding peak value of the neutron transfer coefficient is about 1×10^{-2} per fm/ c which is close to the TDHF calculations in Ref. [59]. The proton transfer coefficients are not sensitive to the symmetry energy in $^{124}\text{Xe} + ^{208}\text{Pb}$ reactions. Because the symmetry energy mainly influences the neutron transport in the case where the projectile and target have a large difference of N/Z values. In addition, we note that the time of neutron transfer starts at $t = 150$ fm/ c which is earlier than that of proton transfer. This is due to the fact that the proton transfer is prevented by a high barrier between the reaction partners at the early stages of the collisions [see Figs. 2(a) and 2(c)].

In MNT reactions, the contact time between the reaction partners is related to the collision mode. Different collision mechanisms can be distinguished by analyzing the TKE-

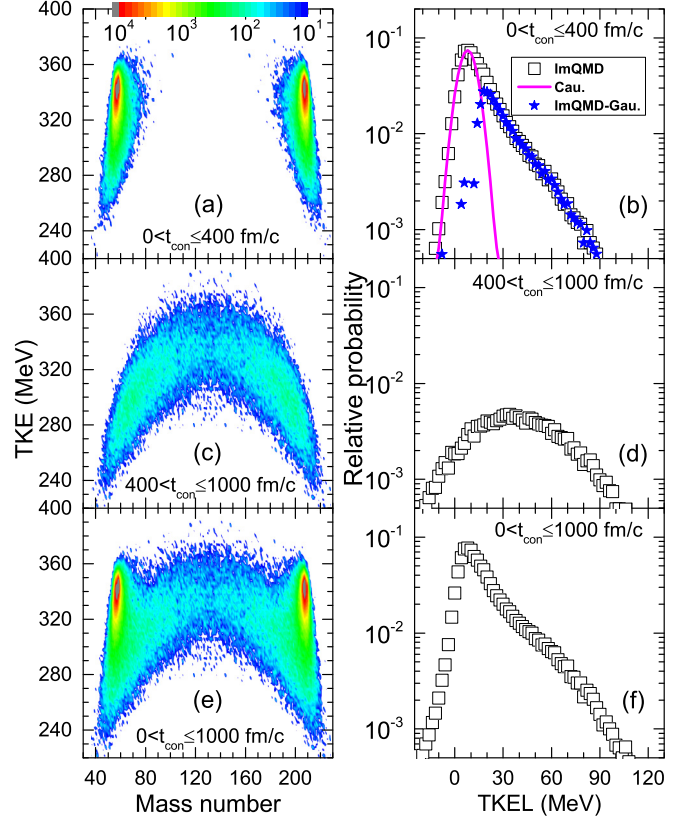


FIG. 6. Left panels: TKE-Mass distributions of primary binary fragments in $^{58}\text{Ni} + ^{208}\text{Pb}$ at $E_{\text{lab}} = 345$ MeV for the contact time ranges of $0 < t_{\text{con}} \leq 400$, $400 < t_{\text{con}} \leq 1000$, and $0 < t_{\text{con}} \leq 1000$ fm/ c . The right panels are corresponding TKEL distributions. In (b), the solid line is the quasielastic (Gaussian-like) contribution; stars are the differences between the ImQMD calculations and the Gaussian distribution.

Mass distribution combined with the TKEL distribution of the products. In Fig. 6, we show the TKE-Mass distributions and corresponding TKEL distributions of primary binary fragments in $^{58}\text{Ni} + ^{208}\text{Pb}$ at $E_{\text{lab}} = 345$ MeV for the contact time ranges of $0 < t_{\text{con}} \leq 400$, $400 < t_{\text{con}} \leq 1000$, and $0 < t_{\text{con}} \leq 1000$ fm/ c . The contour plots show the counts of the fragments in logarithmic scale. The region of the impact parameters in calculations is from 0 to b_{max} fm. The quasielastic and the deep-inelastic collisions occur when the contact time is less than 400 fm/ c . As shown in Fig. 6(b), the quasielastic collision events can be extracted through fitting the peak of the TKEL distribution by a Gaussian curve. In general, the contact time between the reaction partners for the quasielastic collision events is shorter than that for the deep-inelastic collision events. There are only a few nucleon transfers between the projectile and target. One can see that the TKEL of the quasielastic collision events is less than 30 MeV. The differences between the ImQMD calculations and Gaussian curve are mainly the deep-inelastic collision events. Most of the quasifission events occur at $400 < t_{\text{con}} \leq 1000$ fm/ c . The masses distribute in a rather broad range. There are a large number of nucleon transfers, which may lead

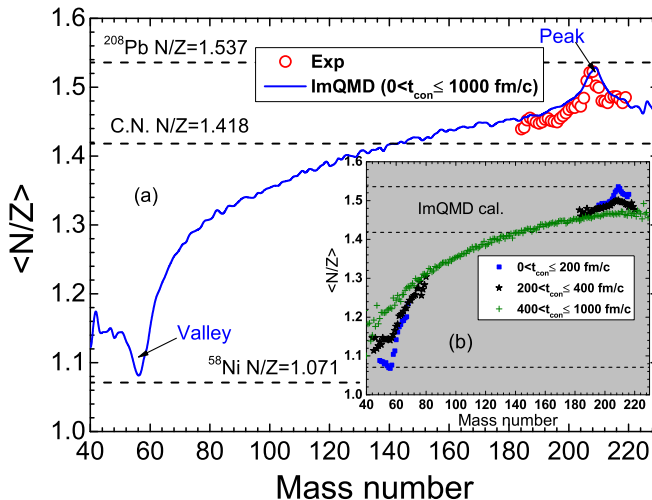


FIG. 7. (a) Average N/Z values for primary binary products of $^{58}\text{Ni} + ^{208}\text{Pb}$ at $E_{\text{lab}} = 345$ MeV. The solid line denotes the calculations of the ImQMD model with $0 < t_{\text{con}} \leq 1000$ fm/ c . The dashed lines indicate the N/Z values of the projectile, the target, and the compound nucleus. The elastic scattering and fusion-fission events are not included. The experimental data (open circles) are reconstructed primary fragments taken from Ref. [18]. (b) Calculated average N/Z values of the primary binary products with contact time ranges of $0 < t_{\text{con}} \leq 200$, $200 < t_{\text{con}} \leq 400$, and $400 < t_{\text{con}} \leq 1000$ fm/ c .

to the isospin equilibration between the quasiprojectile and quasitarget fragments.

The average N/Z values of the primary products in $^{58}\text{Ni} + ^{208}\text{Pb}$ at $E_{\text{lab}} = 345$ MeV are shown in Fig. 7. The solid line in Fig. 7(a) denotes the calculations of the ImQMD model with $0 < t_{\text{con}} \leq 1000$ fm/ c in the region of the impact parameters from 0 to b_{max} fm. The elastic scattering and fusion-fission events are not taken into account. The N/Z values of the projectile, the target, and the compound nucleus are 1.071, 1.537, and 1.418, respectively. From Fig. 7(a), one sees that the experimental data can be reasonably well reproduced by the ImQMD calculations. The average N/Z values of the projectile-like products increase rapidly with increasing nucleon transfer due to the isospin transport from the target to projectile. On the curve, a steep valley and a peak can be clearly seen in the vicinity of the projectile and target. This feature was also found in the reactions of $^{64}\text{Ni} + ^{130}\text{Te}$ and $^{64}\text{Ni} + ^{208}\text{Pb}$ [18,43]. In fact, the isospin equilibration process depends strongly on the contact time of the reaction partners. Figure 7(b) shows the average N/Z values of the primary products with contact time regions of $0 < t_{\text{con}} \leq 200$, $200 < t_{\text{con}} \leq 400$, and $400 < t_{\text{con}} \leq 1000$ fm/ c . In the case of $0 < t_{\text{con}} \leq 200$ fm/ c , most of the primary products are produced in the quasielastic collisions. The strong neutron flow from

the target to projectile results in a sharp increase of N/Z values of the projectile-like fragments. However, the system cannot reach the situation of complete isospin equilibration due to a short contact time. With increasing contact time, the enhanced effect of the isospin equilibration can be seen clearly. The products of complete isospin equilibration are produced in symmetric quasifission reactions. The isospin equilibration process in the MNT reactions can result in the production of very neutron-rich projectile-like fragments. A strong absorption of neutrons by the projectile (^{58}Ni) was observed by the experiment [18]. For example, after neutron evaporation, ^{67}Ni with a production cross section of about 15 μb has been detected in the $\gamma-\gamma$ coincidence analysis.

IV. CONCLUSIONS

In summary, the production cross sections of isotopes in the reaction of $^{58}\text{Ni} + ^{208}\text{Pb}$ at $E_{\text{lab}} = 328.4$ MeV are calculated by the ImQMD model. The results show that the ImQMD model is suitable to describe the MNT reactions at near-barrier energies. The isospin equilibration process in $^{124}\text{Xe} + ^{208}\text{Pb}$ at head-on collisions is studied. The values of the isospin asymmetry in the cores of two reaction partners are uniform during the collisions. The neutrons are preferably driven to the low-density area. On the surface of the nuclei, the value of isospin asymmetry is larger than the core of the nuclei. The direction of neutron flow is from the target to projectile along the low-density path. And the neutrons transfer process is very sensitive to the symmetry energy. The neutron flow is enhanced under the large symmetry energy coefficient. The isospin equilibration process depends strongly on the contact time of the reaction partners. By analyzing the average N/Z values of the primary binary products in $^{58}\text{Ni} + ^{208}\text{Pb}$ at $E_{\text{lab}} = 345$ MeV, we find that the average N/Z values of the projectile-like products increase rapidly with increasing nucleon transfer. In the quasielastic collisions, the system cannot reach the situation of complete isospin equilibration due to a short contact time. The complete isospin equilibration process is noticed in symmetric quasifission reactions where there are a massive transfer of nucleons and large energy dissipation.

ACKNOWLEDGMENTS

This work was supported by the National Natural Science Foundation of China under Grants No. 11805015, No. 11635003, No. 11025524, No. 11161130520, and No. 11605270; the National Basic Research Program of China under Grant No. 2010CB832903; the European Commission's 7th Framework Programme (Fp7-PEOPLE-2010-IRSES) under Grant Agreement Project No. 269131; the project funded by China Postdoctoral Science Foundation (Grants No. 2016M600956 and No. 2018T110069); the Beijing Postdoctoral Research Foundation (2017-zz-076).

[1] M. B. Tsang, T. X. Liu, L. Shi, P. Danielewicz, C. K. Gelbke, X. D. Liu, W. G. Lynch, W. P. Tan, G. Verde, A. Wagner, H. S. Xu, W. A. Friedman, L. Beaulieu, B. Davin, R. T. de

Souza, Y. Larochelle, T. Lefort, R. Yanez, V. E. Viola, Jr., R. J. Charity, and L. G. Sobotka, *Phys. Rev. Lett.* **92**, 062701 (2004).

- [2] V. Baran, M. Colonna, M. Di Toro, M. Zielinska-Pfabé, and H. H. Wolter, *Phys. Rev. C* **72**, 064620 (2005).
- [3] I. Lombardo, C. Agodi, R. Alba, F. Amorini, A. Anzalone, I. Berceanu, G. Cardella, S. Cavallaro, M. B. Chatterjee, E. De Filippo, A. Di Pietro, P. Figuera, E. Geraci, G. Giuliani, L. Grassi, A. Grzeszczuk, J. Han, E. La Guidara, G. Lanzalone, N. Le Neindre, C. Maiolino, A. Pagano, M. Papa, S. Pirrone, G. Politi, A. Pop, F. Porto, F. Rizzo, P. Russotto, D. Santonocito, and G. Verde, *Phys. Rev. C* **82**, 014608 (2010).
- [4] D. D. S. Coupland, W. G. Lynch, M. B. Tsang, P. Danielewicz, and Y. X. Zhang, *Phys. Rev. C* **84**, 054603 (2011).
- [5] J. Su, L. Zhu, and C. C. Guo, *Phys. Lett. B* **782**, 682 (2018).
- [6] Z. Y. Sun, M. B. Tsang, W. G. Lynch, G. Verde, F. Amorini, L. Andronenko, M. Andronenko, G. Cardella, M. Chatterje, P. Danielewicz, E. De Filippo, P. Dinh, E. Galichet, E. Geraci, H. Hua, E. La Guidara, G. Lanzalone, H. Liu, F. Lu, S. Lukyanov, C. Maiolino, A. Pagano, S. Piantelli, M. Papa, S. Pirrone, G. Politi, F. Porto, F. Rizzo, P. Russotto, D. Santonocito, and Y. X. Zhang, *Phys. Rev. C* **82**, 051603(R) (2010).
- [7] E. Galichet, M. F. Rivet, B. Borderie, M. Colonna, R. Bougault, A. Chbihi, R. Dayras, D. Durand, J. D. Frankland, D. C. R. Guinet, P. Lautesse, N. Le Neindre, O. Lopez, L. Manduci, M. Parlog, E. Rosato, B. Tamain, E. Vient, C. Volant, and J. P. Wieleczko, *Phys. Rev. C* **79**, 064614 (2009).
- [8] E. Galichet, M. Colonna, B. Borderie, and M. F. Rivet, *Phys. Rev. C* **79**, 064615 (2009).
- [9] S. Barlini, S. Piantelli, G. Casini, P. R. Maurenzig, A. Olmi, M. Bini, S. Carboni, G. Pasquali, G. Poggi, A. A. Stefanini, R. Bougault, E. Bonnet, B. Borderie, A. Chbihi, J. D. Frankland, D. Gruyer, O. Lopez, N. Le Neindre, M. Parlog, M. F. Rivet, E. Vient, E. Rosato, G. Spadaccini, M. Vigilante, M. Bruno, T. Marchi, L. Morelli, M. Cinausero, M. Degerlier, F. Gramagna, T. Kozik, T. Twaróg, R. Alba, C. Maiolino, and D. Santonocito, *Phys. Rev. C* **87**, 054607 (2013).
- [10] M. Di Toro, A. Olmi, and R. Roy, *Eur. Phys. J. A* **30**, 65 (2006).
- [11] R. Lionti, V. Baran, M. Colonna, and M. Di Toro, *Phys. Lett. B* **625**, 33 (2005).
- [12] T. Welsh, W. Loveland, R. Yanez, J. S. Barrett, E. A. McCutchan, A. A. Sonzogni, T. Johnson, S. Zhu, J. P. Greene, A. D. Ayangeakaa, M. P. Carpenter, T. Lauritsen, J. L. Harker, W. B. Walters, B. M. S. Amro, and P. Coppe, *Phys. Lett. B* **771**, 119 (2017).
- [13] J. S. Barrett, W. Loveland, R. Yanez, S. Zhu, A. D. Ayangeakaa, M. P. Carpenter, J. P. Greene, R. V. F. Janssens, T. Lauritsen, E. A. McCutchan, A. A. Sonzogni, C. J. Chiara, J. L. Harker, and W. B. Walters, *Phys. Rev. C* **91**, 064615 (2015).
- [14] Y. X. Watanabe, Y. H. Kim, S. C. Jeong, Y. Hirayama, N. Imai, H. Ishiyama, H. S. Jung, H. Miyatake, S. Choi, J. S. Song, E. Clement, G. de France, A. Navin, M. Rejmund, C. Schmitt, G. Pollarolo, L. Corradi, E. Fioretto, D. Montanari, M. Niikura, D. Suzuki, H. Nishibata, and J. Takatsu, *Phys. Rev. Lett.* **115**, 172503 (2015).
- [15] O. Beliuskina, S. Heinz, V. Zagrebaev, V. Comas, C. Heinz, S. Hofmann, R. Knöbel, M. Stahl, D. Ackermann, F. P. Heßberger, B. Kindler, B. Lommel, J. Maurer, and R. Mann, *Eur. Phys. J. A* **50**, 161 (2014).
- [16] V. F. Comas, S. Heinz, S. Hofmann, D. Ackermann, J. A. Heredia, F. P. Heßberger, J. Khuyagbaatar, B. Kindler, B. Lommel, and R. Mann, *Eur. Phys. J. A* **49**, 112 (2013).
- [17] E. M. Kozulin, E. Vardaci, G. N. Knyazheva, A. A. Bogachev, S. N. Dmitriev, I. M. Itkis, M. G. Itkis, A. G. Knyazev, T. A. Loktev, K. V. Novikov, E. A. Razinkov, O. V. Rudakov, S. V. Smirnov, W. Trzaska, and V. I. Zagrebaev, *Phys. Rev. C* **86**, 044611 (2012).
- [18] W. Królas, R. Broda, B. Fornal, T. Pawłat, J. Wrzesiński, D. Bazzacco, G. de Angelis, S. Lunardi, R. Menegazzo, D. R. Napoli, and C. Rossi Alvarez, *Nucl. Phys. A* **832**, 170 (2010).
- [19] A. Vogt, B. Birkenbach, P. Reiter, L. Corradi, T. Mijatović, D. Montanari, S. Szilner, D. Bazzacco, M. Bowry, A. Bracco, B. Bruyneel, F. C. L. Crespi, G. de Angelis, P. Désesquelles, J. Eberth, E. Farnea, E. Fioretto, A. Gadea, K. Geibel, A. Gengelbach, A. Giaz, A. Görgen, A. Gottardo, J. Grebosz, H. Hess, P. R. John, J. Jolie, D. S. Judson, A. Jungclaus, W. Korten, S. Leoni, S. Lunardi, R. Menegazzo, D. Mengoni, C. Michelagnoli, G. Montagnoli, D. Napoli, L. Pellegrini, G. Pollarolo, A. Pullia, B. Quintana, F. Radeck, F. Recchia, D. Rosso, E. Şahin, M. D. Salsac, F. Scarlassara, P.-A. Söderström, A. M. Stefanini, T. Steinbach, O. Stezowski, B. Szpak, Ch. Theisen, C. Ur, J. J. Valiente-Dobón, V. Vandone, and A. Wiens, *Phys. Rev. C* **92**, 024619 (2015).
- [20] T. Mijatović, S. Szilner, L. Corradi, D. Montanari, G. Pollarolo, E. Fioretto, A. Gadea, A. Goasduff, D. J. Malenica, N. Mărginean, M. Milin, G. Montagnoli, F. Scarlassara, N. Soić, A. M. Stefanini, C. A. Ur, and J. J. Valiente-Dobón, *Phys. Rev. C* **94**, 064616 (2016).
- [21] M. V. Pajtler, S. Szilner, L. Corradi, G. de Angelis, E. Fioretto, A. Gadea, F. Haas, S. Lunardi, D. Jelavić Malenica, N. Mărginean, D. Mengoni, T. Mijatović, G. Montagnoli, D. Montanari, G. Pollarolo, F. Recchia, M.-D. Salsac, F. Scarlassara, N. Soić, A. M. Stefanini, C. A. Ur, and J. J. Valiente-Dobón, *Nucl. Phys. A* **941**, 273 (2015).
- [22] L. Corradi, G. Pollarolo, and S. Szilner, *J. Phys. G* **36**, 113101 (2009).
- [23] V. I. Zagrebaev and W. Greiner, *Phys. Rev. Lett.* **101**, 122701 (2008).
- [24] C. Li, P. W. Wen, J. J. Li, G. Zhang, B. Li, X. X. Xu, Z. Liu, S. Zhu, and F. S. Zhang, *Phys. Lett. B* **776**, 278 (2018).
- [25] C. Li, P. W. Wen, J. J. Li, G. Zhang, B. Li, and F. S. Zhang, *Nucl. Sci. Tech.* **28**, 110 (2017).
- [26] H. Yao and N. Wang, *Phys. Rev. C* **95**, 014607 (2017).
- [27] N. Wang and L. Guo, *Phys. Lett. B* **760**, 236 (2016).
- [28] L. Zhu, J. Su, W. J. Xie, and F. S. Zhang, *Phys. Lett. B* **767**, 437 (2017).
- [29] L. Zhu, P. W. Wen, C. J. Lin, X. J. Bao, J. Su, C. Li, and C. C. Guo, *Phys. Rev. C* **97**, 044614 (2018).
- [30] Z. Q. Feng, *Phys. Rev. C* **95**, 024615 (2017).
- [31] K. Zhao, Z. X. Li, Y. X. Zhang, N. Wang, Q. F. Li, C. W. Shen, Y. J. Wang, and X. Z. Wu, *Phys. Rev. C* **94**, 024601 (2016).
- [32] C. Li, F. Zhang, J. J. Li, L. Zhu, J. L. Tian, N. Wang, and F. S. Zhang, *Phys. Rev. C* **93**, 014618 (2016).
- [33] M. Veselsky and G. A. Souliotis, *Nucl. Phys. A* **872**, 1 (2011).
- [34] G. G. Adamian, N. V. Antonenko, V. V. Sargsyan, and W. Scheid, *Phys. Rev. C* **81**, 057602 (2010).
- [35] Yu. E. Penionzhkevich, G. G. Adamian, and N. V. Antonenko, *Phys. Lett. B* **621**, 119 (2005).
- [36] E. M. Kozulin, G. N. Knyazheva, S. N. Dmitriev, I. M. Itkis, M. G. Itkis, T. A. Loktev, K. V. Novikov, A. N. Baranov, W. H. Trzaska, E. Vardaci, S. Heinz, O. Beliuskina, and S. V. Khlebnikov, *Phys. Rev. C* **89**, 014614 (2014).

- [37] E. M. Kozulin, V. I. Zagrebaev, G. N. Knyazheva, I. M. Itkis, K. V. Novikov, M. G. Itkis, S. N. Dmitriev, I. M. Harca, A. E. Bondarchenko, A. V. Karpov, V. V. Saiko, and E. Vardaci, *Phys. Rev. C* **96**, 064621 (2017).
- [38] G. N. Knyazheva, E. M. Kozulin, R. N. Sagaidak, A. Yu. Chizhov, M. G. Itkis, N. A. Kondratiev, V. M. Voskressensky, A. M. Stefanini, B. R. Behera, L. Corradi, E. Fioretto, A. Gadea, A. Latina, S. Szilner, M. Trotta, S. Beghini, G. Montagnoli, F. Scarlassara, F. Haas, N. Rowley, P. R. S. Gomes, and A. Szanto de Toledo, *Phys. Rev. C* **75**, 064602 (2007).
- [39] R. du Rietz, D. J. Hinde, M. Dasgupta, R. G. Thomas, L. R. Gasques, M. Evers, N. Lobanov, and A. Wakhle, *Phys. Rev. Lett.* **106**, 052701 (2011).
- [40] E. Prasad, D. J. Hinde, E. Williams, M. Dasgupta, I. P. Carter, K. J. Cook, D. Y. Jeung, D. H. Luong, C. S. Palshetkar, D. C. Rafferty, K. Ramachandran, C. Simenel, and A. Wakhle, *Phys. Rev. C* **96**, 034608 (2017).
- [41] R. T. de Souza, W. U. Schröder, J. R. Huizinga, R. Planeta, K. Kwiatkowski, V. E. Viola, and H. Breuer, *Phys. Rev. C* **37**, 1783(R) (1988).
- [42] R. Planeta, S. H. Zhou, K. Kwiatkowski, W. G. Wilson, V. E. Viola, H. Breuer, D. Benton, F. Khazaie, R. J. McDonald, A. C. Mignerey, A. Weston-Dawkes, R. T. de Souza, J. R. Huizinga, and W. U. Schröder, *Phys. Rev. C* **38**, 195 (1988).
- [43] W. Królas, R. Broda, B. Fornal, T. Pawłat, H. Grawe, K. H. Maier, M. Schramm, and R. Schubart, *Nucl. Phys. A* **724**, 289 (2003).
- [44] D. Guerreau, J. Galin, B. Gatty, and X. Tarrago, *Z. Phys. A* **295**, 105 (1980).
- [45] N. Wang, Z. X. Li, and X. Z. Wu, *Phys. Rev. C* **65**, 064608 (2002).
- [46] N. Wang, Z. X. Li, X. Z. Wu, J. L. Tian, Y. X. Zhang, and M. Liu, *Phys. Rev. C* **69**, 034608 (2004).
- [47] J. Aichelin, *Phys. Rep.* **202**, 233 (1991).
- [48] M. Papa, T. Maruyama, and A. Bonasera, *Phys. Rev. C* **64**, 024612 (2001).
- [49] G. Giuliani, H. Zheng, and A. Bonasera, *Prog. Part. Nucl. Phys.* **76**, 116 (2014).
- [50] N. Wang, L. Ou, Y. X. Zhang, and Z. X. Li, *Phys. Rev. C* **89**, 064601 (2014).
- [51] J. L. Tian, X. Z. Wu, K. Zhao, Y. X. Zhang, and Z. X. Li, *Phys. Rev. C* **77**, 064603 (2008).
- [52] L. Corradi, A. M. Vinodkumar, A. M. Stefanini, E. Fioretto, G. Prete, S. Beghini, G. Montagnoli, F. Scarlassara, G. Pollarolo, F. Cerutti, and A. Winther, *Phys. Rev. C* **66**, 024606 (2002).
- [53] A. Winther, *Nucl. Phys. A* **572**, 191 (1994).
- [54] A. Winther, *Nucl. Phys. A* **594**, 203 (1995).
- [55] <http://personalpage.esfn.it/~nanni/grazing/>.
- [56] R. J. Charity, *Phys. Rev. C* **82**, 014610 (2010).
- [57] K. Washiyama and D. Lacroix, *Phys. Rev. C* **78**, 024610 (2008).
- [58] S. Ayik, K. Washiyama, and D. Lacroix, *Phys. Rev. C* **79**, 054606 (2009).
- [59] S. Ayik, B. Yilmaz, and O. Yilmaz, *Phys. Rev. C* **92**, 064615 (2015).